Induction of Ca^{2+}-driven apoptosis in chronic lymphocytic leukemia cells by peptide-mediated disruption of Bcl-2–IP_3 receptor interaction

*Fei Zhong,[1] *Michael W. Harr,[1] Geert Bultynck,[2] Giovanni Monaco,[2] Jan B. Parys,[2] Humbert De Smedt,[2] Yi-Ping Rong,[1] Jason K. Molitoris,[1] Minh Lam,[3] Christopher Ryder,[1] Shigemi Matsuyama,[1] and Clark W. Distelhorst[1]

[1]Departments of Medicine and Pharmacology, Case Western Reserve University School of Medicine, Case Comprehensive Cancer Center, and University Hospitals Case Medical Center, Cleveland, OH; [2]Laboratory of Molecular and Cellular Signalling, Department of Molecular and Cellular Biology, K.U. Leuven Campus Gasthuisberg, Leuven, Belgium; and [3]Department of Dermatology, Case Western Reserve University School of Medicine, Case Comprehensive Cancer Center, and University Hospitals Case Medical Center, Cleveland, OH

Bcl-2 contributes to the pathophysiology and therapeutic resistance of chronic lymphocytic leukemia (CLL). Therefore, developing inhibitors of this protein based on a thorough understanding of its mechanism of action is an active and promising area of inquiry. One approach centers on agents (eg, ABT-737) that compete with proapoptotic members of the Bcl-2 protein family for binding in the hydrophobic groove formed by the BH1-BH3 domains of Bcl-2. Another region of Bcl-2, the BH4 domain, also contributes to the antiapoptotic activity of Bcl-2 by binding to the inositol 1,4,5-trisphosphate receptor (IP_3R) Ca^{2+} channel, inhibiting IP_3-dependent Ca^{2+} release from the endoplasmic reticulum. We report that a novel synthetic peptide, modeled after the Bcl-2–interacting site on the IP_3R, binds to the BH4 domain of Bcl-2 and functions as a competitive inhibitor of the Bcl-2–IP_3R interaction. By disrupting the Bcl-2–IP_3R interaction, this peptide induces an IP_3R-dependent Ca^{2+} elevation in lymphoma and leukemia cell lines and in primary CLL cells. The Ca^{2+} elevation evoked by this peptide induces apoptosis in CLL cells, but not in normal peripheral blood lymphocytes, suggesting the involvement of the Bcl-2–IP_3R interaction in the molecular mechanism of CLL and indicating the potential merit of targeting this interaction therapeutically. (*Blood*. 2011;117(10):2924-2934)

Introduction

The Bcl-2 protein contributes to the pathophysiology of cancer and the resistance of cancer to therapeutic agents by virtue of its ability to inhibit apoptosis.[1,2] The Bcl-2–positive lymphoid malignancies follicular lymphoma and chronic lymphocytic leukemia (CLL) are prime examples. They are associated with an elevation of Bcl-2 because of the t(14;18) chromosomal translocation in follicular lymphoma[3] and the loss of miR-15a and miR16-1 in CLL.[4,5] Cure of these malignancies is infrequently achieved with current therapeutic modalities, and thus a major challenge remains to develop new treatment modalities based on an understanding of the fundamental disease mechanisms.[6]

Bcl-2 blocks apoptosis in part by binding its proapoptotic relatives, thus preserving mitochondrial integrity and preventing cytochrome c release.[7,8] Therefore, considerable investment has been made in the development of novel therapeutic agents, such as ABT-737, that disrupt the inhibitory interaction of Bcl-2 with its proapoptotic relatives.[1,2,9-11] Several of these agents are currently undergoing clinical testing. However, Bcl-2 also inhibits apoptosis by regulating the release of Ca^{2+} from the endoplasmic reticulum (ER).[12-14] This recently characterized mechanism involves a physical interaction of Bcl-2 with the inositol 1,4,5-trisphosphate receptor (IP_3R) Ca^{2+}-release channel on the ER. Through this interaction, Bcl-2 prevents cytoplasmic Ca^{2+} elevation sufficient to trigger apoptosis. However, the potential contribution of the Bcl-2–IP_3R interaction to the survival of CLL has not been investigated, so the opportunity for targeting this interaction therapeutically has not yet been realized.

The IP_3R is an IP_3-gated Ca^{2+} channel that is highly conserved, represented by 3 isoforms, and present in virtually all cell types.[15,16] IP_3-dependent release of Ca^{2+} from the ER into the cytoplasm produces Ca^{2+} signals, generally in the form of Ca^{2+} oscillations, which govern diverse cellular functions including cell proliferation and survival.[17,18] Ca^{2+} oscillations support cell survival in part by positively regulating mitochondrial metabolism, but sustained high-amplitude elevations of Ca^{2+} induce mitochondrial Ca^{2+} overload and apoptosis.[19-21] Bcl-2 inhibits high-amplitude, proapoptotic Ca^{2+} elevation but does not interfere with physiologic Ca^{2+} oscillations.[22] In fact, under certain circumstances Bcl-2 and its homolog Bcl-xl enhance Ca^{2+} oscillations,[22-26] and through this mechanism are predicted to promote efficient mitochondrial bioenergetics.[27] Thus, Bcl-2 supports cell survival both by enhancing physiologic Ca^{2+} signals and by blocking proapoptotic Ca^{2+} elevation.

A major focus of our work has been to understand how Bcl-2 inhibits proapoptotic elevation of Ca^{2+} based on evidence that Bcl-2 binds to the IP_3R and thus inhibits ER Ca^{2+} release.[28-32] Although this interaction has been mainly detected in cell extracts by coimmunoprecipitation or blue native gel electrophoresis, we recently confirmed the Bcl-2–IP_3R interaction in living cells using fluorescence resonance energy transfer.[33] Furthermore, our findings indicate that the interaction involves direct binding of the BH4

Submitted September 14, 2010; accepted December 12, 2010. Prepublished online as *Blood* First Edition paper, December 30, 2010; DOI 10.1182/blood-2010-09-307405.

An Inside *Blood* analysis of this article appears at the front of this issue.

The publication costs of this article were defrayed in part by page charge payment. Therefore, and solely to indicate this fact, this article is hereby marked "advertisement" in accordance with 18 USC section 1734.

*F.Z. and M.W.H. contributed equally to this study.

domain of Bcl-2 to the regulatory and coupling domain of the IP_3R.[33,34] This region, located between the IP_3-binding domain at the N-terminus of the IP_3R and the transmembrane channel domain near the C-terminus, binds a variety of regulatory proteins and undergoes several secondary modifications, thus modulating channel opening in response to IP_3 binding.[15,16]

A major tool in our recent investigation of the Bcl-2–IP_3R interaction has been a synthetic peptide, previously referred to as peptide 2 and in the present study as the IP_3R-derived peptide (IDP).[33] The IDP corresponds to a 20–amino acid sequence within the Bcl-2–binding site on the IP_3R and functions as a competitive inhibitor of the Bcl-2–IP_3R interaction.[33,34] By disrupting this interaction, IDP reverses Bcl-2–mediated inhibition of both IP_3-dependent channel opening and IP_3-dependent ER Ca^{2+} release. Thus, when delivered into Bcl-2–positive T cells by fusion with the cell-penetrating peptide of HIV transactivator of transcription (TAT-IDP) or by interaction with Chariot peptide uptake reagent, the IDP reverses Bcl-2–mediated inhibition of IP_3-dependent Ca^{2+} elevation and apoptosis induced by anti-CD3 antibody.[33]

We report the development of a TAT-IDP analog, TAT-$IDP_{DD/AA}$, which induces striking Ca^{2+} elevation in primary CLL cells by binding to the BH4 domain of Bcl-2 and disrupting Bcl-2–IP_3R interaction, thereby triggering Ca^{2+}-dependent apoptosis. These findings suggest a novel approach for targeting Bcl-2 for therapeutic purposes. In addition, the discovery that disrupting the Bcl-2–IP_3R interaction is sufficient to induce IP_3R-mediated Ca^{2+} elevation suggests that Bcl-2 may contribute to the pathophysiology of CLL by suppressing proapoptotic Ca^{2+} signals downstream of constitutively active B-cell receptor (BCR) signals.

Methods

Reagents

Fura-2 AM and Hoechst 33342 were from Invitrogen, pepstatin A from Roche, and ABT-737 from Abbott Laboratories. Peptides were from GenScript and were > 95% pure as shown by mass spectrometry and high-performance liquid chromatography.

Cell culture

WEHI7.2 cells were cultured and stably transfected with expression vectors encoding wild-type Bcl-2 and Bcl-2RS/GG, as described previously.[28,33] Jurkat and RS11846 cells were cultured in RPMI medium supplemented with 10% fetal bovine serum, L-glutamine (2mM), and nonessential amino acids (100μM). Cells were maintained in 5% carbon dioxide at high humidity. DT40 cells were cultured in RPMI medium with 10% fetal bovine serum, 1% chicken serum, and 2mM L-glutamine.

Primary lymphocytes were separated using a Ficoll Hypaque density gradient from the peripheral blood of normal adult volunteers or adult patients with CLL, and suspended in RPMI medium supplemented with 10% fetal bovine serum, L-glutamine (2mM), and nonessential amino acids (100μM) at a density of 2 million cells/mL. B and T cells were separated from normal mononuclear cells by magnetic separation using CD19 microbeads (Miltenyi Biotec). All procedures followed the guidelines and regulations in accordance with internal review board protocol ICC2902/11-02-28 of Case Western Reserve University Cancer Center/University Hospitals of Cleveland Ireland Cancer Center. The use of human subjects in this proposal was approved by the institutional review board of Case Western Reserve University School of Medicine.

Ca^{2+} measurements

Single-cell digital imaging of Fura-2 AM–loaded cells in extracellular buffer (130mM NaCl, 5mM KCl, 1.5mM $CaCl_2$, 1mM $MgCl_2$, 25mM HEPES [N-2-hydroxyethylpiperazine-N′-2-ethanesulfonic acid], pH 7.5, 1 mg/mL of bovine serum albumin, and 5mM glucose) was described previously in detail.[22] Xestospongin C (Enzo Life Sciences International) and U73122 (Sigma), both dissolved in dimethylsulfoxide (DMSO), were added to cells 30 minutes before Ca^{2+} measurements.

Unidirectional $^{45}Ca^{2+}$-flux assay methods were described previously.[34,35] Briefly, this method involves loading nonmitochondrial Ca^{2+} stores in saponin-permeabilized mouse embryonic fibroblast (MEF) cells with $^{45}Ca^{2+}$. Saponin (20 μg/mL) selectively permeabilizes the plasma membrane by its preferential interaction with cholesterol, providing direct access to the intracellular Ca^{2+} stores, and azide prevents $^{45}Ca^{2+}$ uptake by the mitochondria, leaving only the ER as a Ca^{2+} store. IP_3 (3μM)–mediated $^{45}Ca^{2+}$ efflux was then measured as described previously.[34,35] BH4-Bcl2 peptide (40μM), in the presence or absence of the $IDP_{DD/AA}$ peptide (40μM), was added from 4 minutes before IP_3 to 2 minutes after IP_3. Ca^{2+} release was plotted as fractional loss (percentage/2 minutes) as a function of time.

Western blotting and GST pull-down

Western blotting was performed as described previously.[33] The following antibodies were used: anti–human Bcl-2 (551052; BD Biosciences), anti–mouse/human Bcl-2 (Santa Cruz Biotechnology), and anti-actin (Sigma). Glutathione *S*-transferase (GST) pull-down methods were described previously in detail,[33] and were used here with these modifications: 3xFLAG-Bcl-2 was expressed in COS-7 cells; mutant GST-IP_3R1 domain 3, in which $Asp^{1403}Asp^{1404}$ residues were mutated to Ala, was tested; and glutathione-Sepharose beads were washed 4 times with modified interaction buffer (150 instead of 300mM NaCl without bovine serum albumin), and GST-fusion proteins were eluted by incubating beads with 40 μL of LDS (Invitrogen) for 3 minutes at 95°C. 3xFLAG-tagged Bcl-2 was detected by Western blotting using a mouse monoclonal ANTI-FLAG M2-Peroxidase antibody (Sigma). Total protein content was visualized by GelCode blue (ThermoFisher Scientific) staining of the blot after film development. Quantification was done with ImageJ software Version 1.43u (National Institutes of Health; publisher, Wayne Rasband).

SPR

Binding of GST-Domain3, GST-Domain3DD/AA, and parental GST to the BH4 domain of Bcl-2 was analyzed by surface plasmon resonance (SPR) at 25°C using a Biacore 2000 instrument. Fusion proteins were affinity purified and dialyzed against phosphate-buffered saline (PBS) using a Slide-A-Lyzer with a cutoff of 3 kDa (Pierce) to minimize buffer effect. Fusion protein concentration was determined using bicinchoninic acid protein assay reagent (Pierce), and the quality and integrity were examined by sodium dodecyl sulfate-polyacrylamide gel electrophoresis and GelCode blue (Pierce). Equal amounts (200 ng or 58.2 pmol of biotinylated peptide) of > 80% pure biotinylated BH4-Bcl2 peptide (Biotin-RTGYDNREIVM-KYIHYKLSQRGYEW) and BH4-Bcl2-scrambled peptide (Biotin-WYEKQRSLHGIMYYVIEDRNTKGYR) were immobilized on 2 different flow cells of a streptavidin-coated sensor chip (BR-1000-32; Biacore) using PBS supplemented with 0.005% P20 at pH 7.0. Measurements with GST-fusion proteins as analyte were performed in PBS at a flow rate of 30 μL/min. Different concentrations of the analyte were used in a random order to assess binding (injection volume, 120 μL). Bound peptide was removed by injection of 5 μL of regeneration buffer (25mM NaOH, 0.002% SDS) at 10 μL/min. Background signals were obtained from the reference flow cell containing the BH4–Bcl2-scrambled peptide, and were subtracted to generate response curves using Biaevaluation 3.0 software. Only the association phase of the binding curve was taken into account. Data from 2-3 different sensor grams for each condition were fitted by nonlinear regression analysis to a Hill-Langmuir binding isotherm using Origin 7.0 software.

Coimmunoprecipitation and biotin-streptavidin pull-down

Bcl-2–IP_3R coimmunoprecipitation was performed as described previously.[33] For biotin-streptavidin pull-down experiments, Bcl-2–overexpressing WEHI7.2 cells were incubated on ice for 30 minutes in 400 μL of CHAPS lysis buffer (50mM Tris-HCl, pH 7.5,100mM NaCl, 2mM EDTA,1% CHAPS, 50mM NaF, 1mM Na_3VO_4, and the protease inhibitor

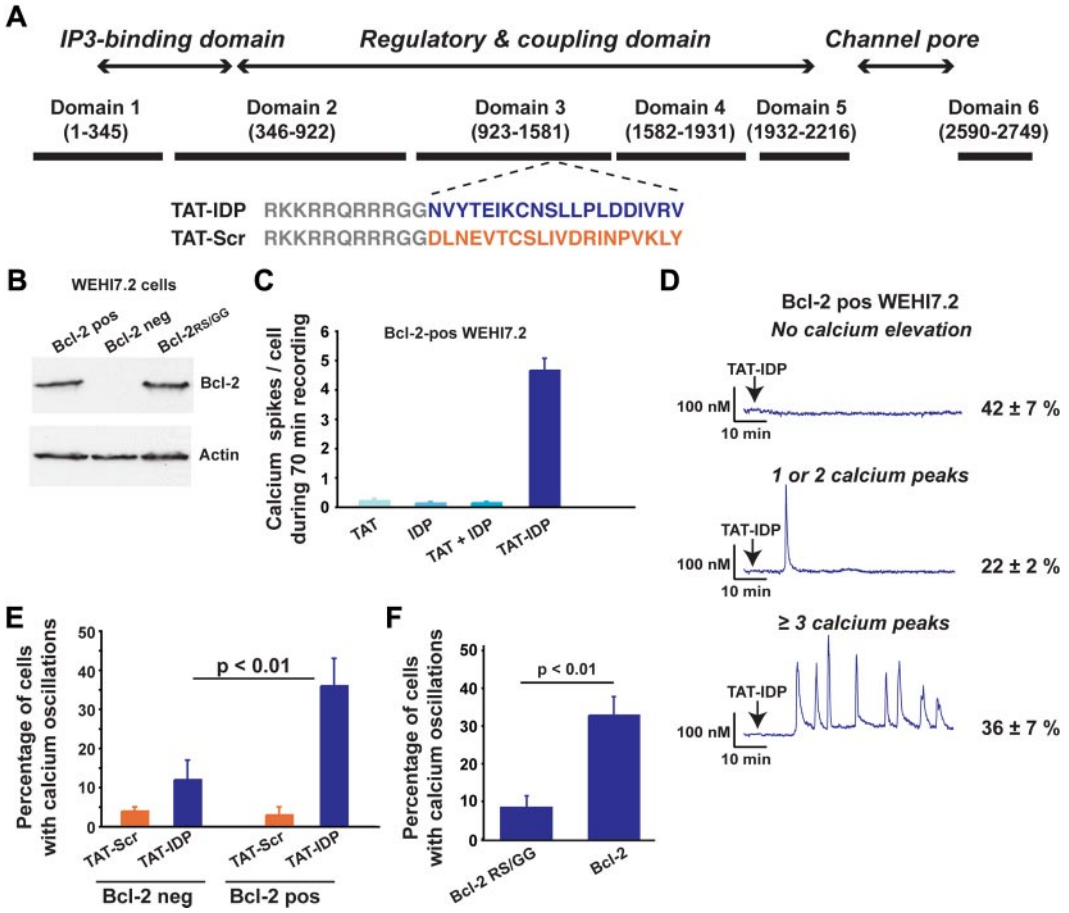

Figure 1. Bcl-2 dependent induction of Ca^{2+} oscillations by TAT-IDP. (A) Diagram of type-1 IP_3R domains designating the origin of the IDP sequence (blue) and the scrambled control sequence (orange), along with the TAT sequence (gray). (B) Immunoblot documenting levels of wild-type and mutant Bcl-2 expressed in Bcl-2–negative WEHI7.2 cells. (C) Number of Ca^{2+} spikes observed per cell in 70 minutes of recordings after adding 2μM of the peptides shown (mean ± SE, 67 cells total). (D) Representative single-cell Ca^{2+} recordings in Bcl-2-positive WEHI7.2 cells (2μM TAT-IDP added at arrow); percentages (mean ± SE) of cells displaying each pattern are based on 3 experiments (90 minutes of recording, average 60 cells per recording). (E) Summary of 2 experiments (mean ± SE) comparing TAT-IDP (2μM)–induced Ca^{2+} responses (90 minutes of recordings, average 60 cells per recording) in Bcl-2–negative versus Bcl-2–positive WEHI7.2 cells. (F) Summary of 3 experiments (mean ± SE) comparing the percentage of cells displaying Ca^{2+} oscillations in response to the addition of 2μM TAT-IDP to WEHI7.2 cells expressing either wild-type Bcl-2 or Bcl-2RS/GG (90 minutes of recording, average 60 cells per recording).

cocktail PhosSTOP). Cell lysates were centrifuged for 15 minutes at 20,000*g* at 4°C, and the supernatant (protein concentration, 5 mg/mL) was continuously rotated with 200μM biotin-Scr or biotin-$IDP_{DD/AA}$ or without peptide at 4°C for 16 hours. Streptavidin-Sepharose beads (40 μL) (Pierce Pull-Down Biotinylated Protein:Protein Interaction Kit, ThermoFisher, Cat no. 21115) were washed 3 times with Tris-buffered saline (25mM Tris-HCl, 0.15M NaCl, pH 7) and then added to 400 μL of cell lysate, followed by rotation for 2 hours at 4°C. The beads were washed 4 times with Tris-buffered saline, centrifuged for 30-60 seconds each time, and then incubated for 3-5 minutes at room temperature with 50 μL of elution buffer provided by the Pierce pull-down kit, and centrifuged at 1250*g* for 30-60 seconds. The supernatant was boiled in sodium dodecyl sulfate-polyacrylamide gel electrophoresis sample buffer for 5 minutes, and Western blotting for Bcl-2 was performed as described in Western blotting section (above).

Apoptosis assays

Trypan blue dye uptake was detected by light microscopy, and propidium iodide uptake was quantified by flow cytometry in association with the annexin V measurements using an FACSAria flow cytometer (Beckman Coulter). Flow cytometric data were analyzed using FlowJo Version 8.8.4 for Macintosh (TreeStar). Apoptotic nuclei were quantified in Hoechst 33342–stained cells by epifluorescence microscopy (Zeiss Axiovert S100) using a 63× fluorescent oil objective (Carl Zeiss) and a Hamumatsu Orca camera at room temperature. The activities of caspase-3 and caspase-7 were measured with the Caspase-Glo 3/7 luminescence assay (Promega) according to the manufacturer's protocol. To monitor mitochondrial membrane potential, cells were incubated with 20nM tetramethyl-rhodamine methyl ester for 20 minutes at 37°C, washed twice with extracellular buffer (see "CA^{2+} measurements" above), and resuspended in extracellular buffer before adding peptides. Confocal images were acquired with an UltraVIEW VoX spinning disc confocal system (Perkin-Elmer) mounted on a Leica DMI6000B microscope equipped with an HCX PL APO 100×/1.4 oil-immersion objective. Tetramethyl-rhodamine methyl ester fluorescence was excited at 561 nm, and its emission was collected using a 580-650 nm bandpass filter.

Statistical analysis

A Student *t* test was used to assess statistical differences between groups. A 2-tailed *P* value of .05 was the threshold for significance. Statistical tests were performed using Microsoft Excel 2004 for Macintosh.

Results

TAT-IDP alone induces Ca^{2+} oscillations in Bcl-2–expressing lymphoma cell lines

Four cell lines, representing lymphoid malignancies of both T- and B-cell origin, were used as shown in Figures 1-4 to lay the

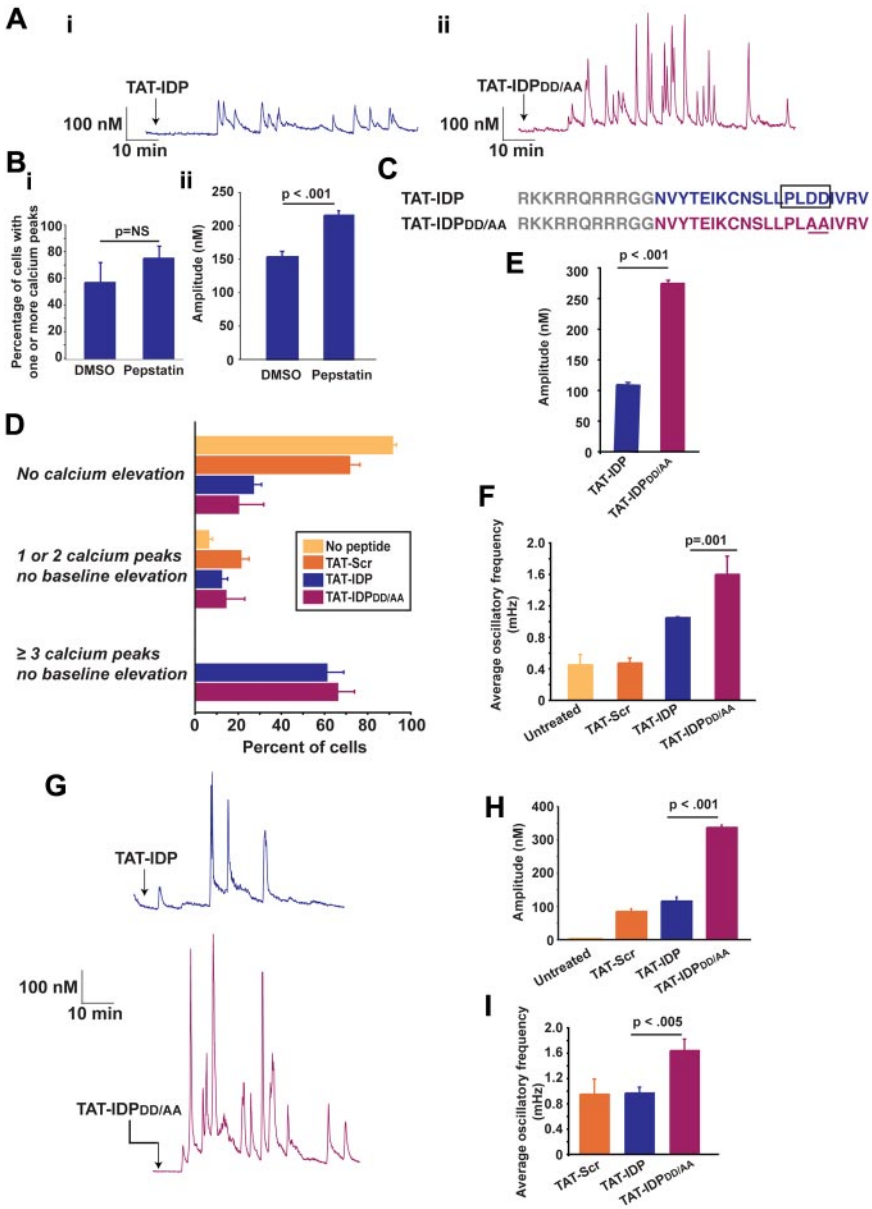

Figure 2. IDP-induced Ca^{2+} oscillations in Jurkat T cells and RS11846 B cells. (A) Single-cell Ca^{2+} recordings showing representative examples of Ca^{2+} oscillations induced by 10μM TAT-IDP or TAT-$IDP_{DD/AA}$ in more than 50% of Jurkat cells (arrow, peptide addition). (B) Enhancement of TAT-IDP–induced Ca^{2+} elevation by treating Jurkat cells with 2μM pepstatin A for 45 minutes before peptide addition: (i) percentage of cells with Ca^{2+} elevation in response to 10μM TAT-IDP in the presence of DMSO or pepstatin A (mean ± SE, 3 experiments, average 78 cells per treatment per experiment); (ii) amplitude of Ca^{2+} spikes induced by 10μM TAT-IDP (mean ± SE, amplitude of 130 spikes observed in a total of 83 DMSO-treated cells and 299 spikes in a total of 73 pepstatin A-treated cells). (C) Peptide sequences showing the predicted aspartyl protease cleavage site in TAT-IDP and its elimination by the DD/AA substitution in TAT-$IDP_{DD/AA}$. (D) Percentage of Jurkat cells displaying each of 3 Ca^{2+} response patterns when untreated or when treated with 10μM TAT-Scr, TAT-IDP, or TAT-$IDP_{DD/AA}$ (mean ± SE, 6 experiments, average of 80 cells analyzed by 90 minutes of single-cell digital imaging per peptide treatment per experiment). (E) Amplitude of Ca^{2+} spikes during 90 minutes of recordings after 10μM peptide addition to Jurkat cells (mean ± SE, 3 experiments, average 85 cells per peptide addition per experiment). (F) Average Ca^{2+} oscillatory frequency in untreated and peptide-treated Jurkat cells based on analysis of 90 minutes of recordings (mean ± SE, 3 experiments, average 85 cells per peptide treatment per experiment). (G) Single-cell Ca^{2+} recordings showing representative examples of Ca^{2+} oscillations induced by 10μM TAT-IDP or TAT-$IDP_{DD/AA}$ in more than 50% of RS11846 cells (arrow, peptide addition). (H) Amplitude of individual Ca^{2+} peaks observed in untreated cells and cells treated with 10μM of each peptide (mean ± SE; no spikes in untreated; 34 spikes with TAT-Scr; 104 spikes with TAT-IDP; 248 spikes with TAT-$IDP_{DD/AA}$). (I) Frequency of Ca^{2+} oscillations induced by 10μM of each peptide in same dataset analyzed in panel H.

foundation for studies using primary CLL cells shown in Figures 5 and 6. The sequence of TAT-IDP and its scrambled control analog, TAT-Scr, are shown in Figure 1A, together with a diagram pinpointing the IP_3R region from which the IDP sequence was derived. Also shown is an immunoblot documenting that Bcl-2 is virtually undetectable in the WEHI7.2 murine T-cell lymphoma line and that Bcl-2 levels are similar in WEHI7.2 cells expressing wild-type Bcl-2 or mutant Bcl-2RS/GG, in which arginine 6 and serine 7 are both converted to glycine (Figure 1B). We demonstrated previously that wild-type Bcl-2 interacts with the IP_3R in these cells, whereas the Bcl-2RS/GG does not.[33] In experiments summarized in Figure 1C, Ca^{2+} elevations were induced when Bcl-2–positive WEHI7.2 cells were treated with TAT-IDP, whereas Ca^{2+} elevations were very infrequent after treatment with TAT alone, IDP alone, or a mixture of TAT and IDP. IDP also induced Ca^{2+} elevations when introduced into the same cells with Chariot peptide uptake reagent (data not shown). The pattern of Ca^{2+} elevation induced by TAT-IDP in Bcl-2–positive WEHI7.2 cells was analyzed by single-cell digital imaging in a large number of experiments (Figure 1D). Two patterns were arbitrarily defined: 1 or 2 isolated Ca^{2+} oscillations were observed in 22% ± 2% of cells, whereas a sustained pattern of Ca^{2+} oscillations (3 or more peaks) was observed in 36% ± 7% of the cells. Thus, on average, more than 50% of Bcl-2–positive cells reproducibly displayed Ca^{2+} elevations in response to TAT-IDP, whereas TAT-Scr did not induce Ca^{2+} elevation to a significant degree. Cell viability was not lost after TAT-IDP treatment (data not shown). Moreover, TAT-IDP did not induce Ca^{2+} elevations to nearly the same degree in Bcl-2–negative cells or Bcl-2RS/GG–positive cells as in cells expressing wild-type Bcl-2 (Figure 1E-F). In summary, these findings indicate that IDP induced Ca^{2+} oscillations when introduced into cells either by fusion with the cell-penetrating peptide TAT or with a commercial peptide uptake reagent, and that this process was dependent on Bcl-2.

TAT-$IDP_{DD/AA}$ is a more effective inducer of Ca^{2+} oscillations than TAT-IDP

TAT-IDP also induces Ca^{2+} oscillations in the Jurkat human T-cell leukemia line (Figure 2A subpanel i), which natively expresses

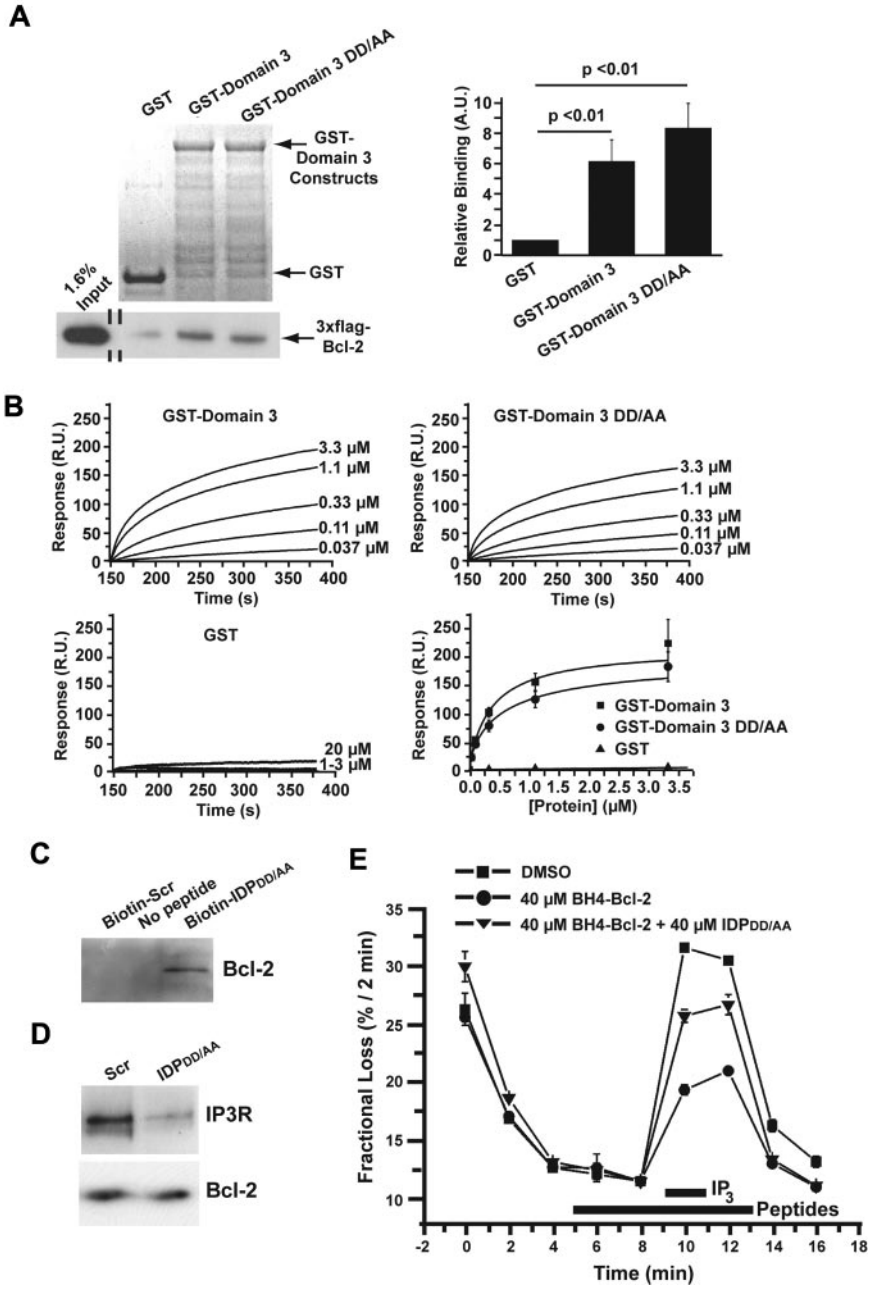

Figure 3. Biochemical and functional characterization of the DD/AA substitution. (A) Typical GST pull-down experiment documenting the binding of 3xFLAG-Bcl-2 in COS-7 cell lysate to GST-Domain3 and GST-Domain3DD/AA using GST as a negative control. GelCode blue–stained membrane showing the presence of GST and the GST-fusion proteins, 7.5 μg each, in the pull-down assay are shown in the top left panel. Immunoblot using an anti-FLAG antibody coupled to horseradish peroxidase to detect 3xFLAG-Bcl-2 both in the input lane and in the pull-down lanes is shown in the bottom left panel. Quantitative analysis of the binding of 3xFLAG-Bcl-2 to GST, GST-Domain3, and GST-Domain3DD/AA by densitometry (ImageJ software) is shown in the right panel. Results (mean ± SE, 4 experiments) were normalized for the binding of 3xFLAG-Bcl-2 to GST. 3xFLAG-Bcl-2 displayed significant binding to both GST-Domain3 and GST-Domain3DD/AA ($P < .01$). (B) SPR demonstrating the binding of both GST-domain3 and GST-domain3DD/AA with a biotin-tagged peptide corresponding to the BH4 domain of Bcl-2 (biotin-BH4-Bcl-2). Typical sensor grams illustrating the association phase of the binding of different concentrations of GST-Domain3 (top left), GST-Domain3DD/AA (top right), and GST (bottom left) to Biotin-BH4-Bcl-2 immobilized to a streptavidin-coated sensor chip. All GST-fusion proteins were dialyzed against the interaction buffer (PBS) to minimize the buffer effect. Values were corrected for background binding of the GST-fusion proteins to Biotin-BH4-Bcl-2reverse. Resonance units (R.U.) increased with increasing concentrations of GST-Domain3 (0.037-3.3μM) or GST-Domain3DD/AA (0.037-3.3μM), but not with increasing concentrations of GST (1-20μM). Quantitative analysis of the background-corrected R.U. signals plotted as mean ± SE obtained from 3 independent experiments (bottom right), in which different concentrations of GST-Domain3, GST-Domain3DD/AA, and GST were applied to the BH4-Bcl-2-coated sensor chip. The data points obtained from GST-Domain3 and GST-Domain3$_{DD/AA}$ were fitted using Origin 7.0 software by a Hill equation, yielding apparent KDs of 0.37 ± 0.13μM and 0.57 ± 0.4μM, respectively. (C) Binding of IDP$_{DD/AA}$ to Bcl-2 demonstrated by biotin-streptavidin pull-down of Bcl-2 from lysate of WEHI7.2 cells overexpressing wild-type Bcl-2. Cell lysate was incubated with or without the indicated peptides for 16 hours, followed by incubation with streptavidin-coated beads. Bcl-2 bound to the beads via biotin-tagged IDP$_{DD/AA}$ was detected by immunoblotting. Results are representative of 3 separate experiments with the same result. (D) Disruption of Bcl-2-IP$_3$R interaction by IDP$_{DD/AA}$. Bcl-2 was immunoprecipitated from lysates of WEHI7.2 cells overexpressing wild-type Bcl-2. Immunoprecipitated proteins were analyzed by immunoblotting for IP$_3$R3 and Bcl-2. (E) IDP$_{DD/AA}$ prevents the inhibition of IP$_3$R-mediated Ca^{2+} release by BH4-Bcl-2, a peptide corresponding to the BH4 domain Bcl-2. A typical unidirectional $^{45}Ca^{2+}$-efflux experiment showing the Ca^{2+} release induced by 3μM IP$_3$ from permeabilized $^{45}Ca^{2+}$-loaded wild-type MEF cells in the presence of vehicle (■), 40μM BH4-Bcl-2 peptide (●), 40μM BH4-Bcl-2 peptide and 40μM IDP$_{DD/AA}$ (▲). All peptides were incubated from 4 minutes before the addition of IP$_3$ to 2 minutes after its addition (bars). Data points of a representative experiment, plotted as fractional loss (percentage/2 minutes) as a function of time, were obtained in duplicate and represent mean ± SD.

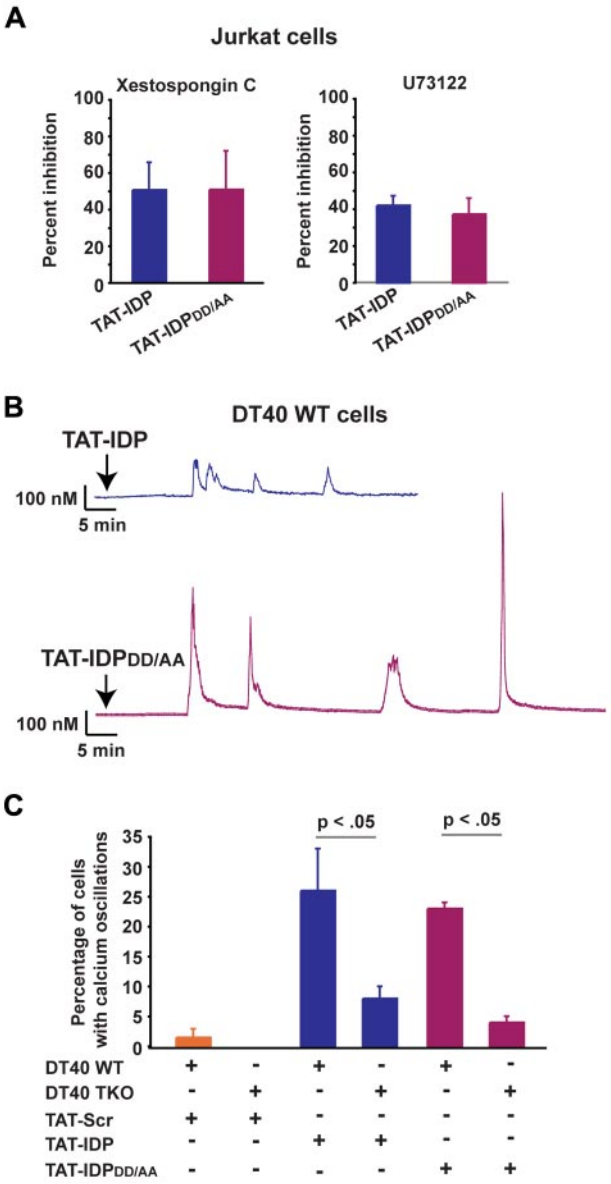

Figure 4. IP_3R dependence of Ca^{2+} oscillations induced by TAT-IDP and TAT-$IDP_{DD/AA}$. (A) Percent inhibition of peptide (10μM)–induced Ca^{2+} oscillations by the IP_3R inhibitor xestospongin C (10μM) or the phospholipase C inhibitor U73122 (0.25μM) in Jurkat cells, based on the percentage of cells displaying Ca^{2+} oscillations during 90 minutes of single-cell recordings (mean ± SE, 3 experiments, average 85 cells analyzed per treatment condition per experiment). (B) Representative single-cell Ca^{2+} recordings illustrating Ca^{2+} responses to 5μM peptide addition (arrow) in wild-type DT40 cells. (C) Percentage of wild-type (WT) and TKO DT40 cells displaying Ca^{2+} oscillations in response to treatment with 5μM peptides (mean ± SE, 4 experiments, average 60 cells analyzed per recording).

Bcl-2 and in which we have previously documented interaction of endogenous Bcl-2 with the IP_3R.[33] TAT-linked peptides are delivered into cells by macropinocytosis[36] and are therefore exposed to endocytic proteases, mainly cathepsins.[37] Moreover, the presence of an aspartyl protease cleavage site, PLDD, in IDP was predicted by 2 algorithms (CLC Main Workbench and the CASVM server[38]). The possibility that TAT-IDP may be subject to degradation when delivered into Jurkat cells was also suggested by a slight, but not significant, increase in both the percentage of cells displaying peptide-induced Ca^{2+} elevations (Figure 2B subpanel i) and a significant enhancement of the amplitude of these Ca^{2+} elevations (Figure 2B subpanel ii) after pretreatment with the aspartyl protease inhibitor pepstatin A. Therefore, an IDP analog, TAT-$IDP_{DD/AA}$ was generated with the goal of eliminating the predicted protease cleavage site (Figure 2C). Representative Ca^{2+} oscillations induced by TAT-$IDP_{DD/AA}$ are shown in Figure 2A (subpanel ii). TAT-IDP and TAT-$IDP_{DD/AA}$ induced Ca^{2+} oscillations in a similar percentage of cells (Figure 2D), but both the amplitude (Figure 2A and E) and frequency (Figure 2A and F) of Ca^{2+} oscillations were much higher with TAT-$IDP_{DD/AA}$ than with TAT-IDP. Another peptide analog in which the predicted protease cleavage site is eliminated without altering overall peptide charge, TAT-$IDP_{DD/EE}$, also induced Ca^{2+} oscillations of higher amplitude and frequency, very similar to TAT-$IDP_{DD/AA}$ (data not shown). In addition, the increased activity of TAT-$IDP_{DD/AA}$ compared with TAT-IDP was observed in the RS11846 human B-cell lymphoma line, which has elevated Bcl-2 because of a t(14;18) chromosomal translocation typical of human follicular lymphoma[39] (Figure 2G-I). Thus, the induction of Ca^{2+} oscillations by these peptides is not unique to T lymphocytes.

TAT-$IDP_{DD/AA}$ binds to the BH4 domain of Bcl-2 to disrupt the Bcl-2–IP_3R interaction and induces Ca^{2+} oscillations

Because TAT-$IDP_{DD/AA}$ was significantly more effective at inducing Ca^{2+} oscillations than TAT-IDP, we investigated its mechanism of action at a biochemical level. As shown in GST pull-down experiments in Figure 3A, binding of 3xFLAG-Bcl-2 to GST-Domain3 was not significantly different from the binding to GST-Domain3DD/AA. Furthermore, the binding of these GST-tagged domains to Biotin-BH4-Bcl-2 (a biotin-tagged peptide corresponding to the BH4 domain of Bcl-2) was measured by SPR (Figure 3B). The results indicated that GST-Domain3 and GST-Domain3DD/AA bound specifically to Biotin-BH4-Bcl-2 with similar affinities. In addition, interaction of $IDP_{DD/AA}$ with Bcl-2 was documented by biotin-streptavidin pull-down (Figure 3C), and disruption of the Bcl-2–IP_3R interaction by $IDP_{DD/AA}$ was confirmed in coimmunoprecipitation experiments (Figure 3D). Consistent with these observations, $IDP_{DD/AA}$ reversed the Bcl-2–imposed inhibition of IP_3-induced $^{45}Ca^{2+}$ efflux from the ER when added to cells after $^{45}Ca^{2+}$ loading and permeabilization with saponin, as was shown previously for IDP[34] (Figure 3E).

Finally, the IP_3R inhibitor xestospongin C and the phospholipase C inhibitor U73122 reduced the percentage of cells displaying peptide-induced Ca^{2+} oscillations, providing further evidence that Ca^{2+} responses to both TAT-IDP and TAT-$IDP_{DD/AA}$ were IP_3R dependent (Figure 4A). In addition, each of these peptides induced Ca^{2+} oscillations in the DT40 B-cell lymphoma line, which expresses all 3 IP_3R isoforms (Figure 4B), but the induction of Ca^{2+} oscillations by these peptides was significantly less in triple IP_3R knockout DT40 cells (Figure 4C).

In summary, these findings suggest that the increase in Ca^{2+} responses induced in Bcl-2–positive cell lines by TAT-$IDP_{DD/AA}$ compared with TAT-IDP was likely because of increased cellular uptake and stability as a result of reduced proteolytic cleavage rather than increased affinity of TAT-$IDP_{DD/AA}$ for Bcl-2. In addition, these findings confirm that TAT-$IDP_{DD/AA}$ functions as a competitive inhibitor of the Bcl-2–IP3R interaction, as was shown previously for TAT-IDP.[33]

TAT-$IDP_{DD/AA}$ induces a striking Ca^{2+} elevation in primary CLL cells

The effects of these peptides were next investigated in primary CLL cells, chosen for this purpose because CLL is invariably

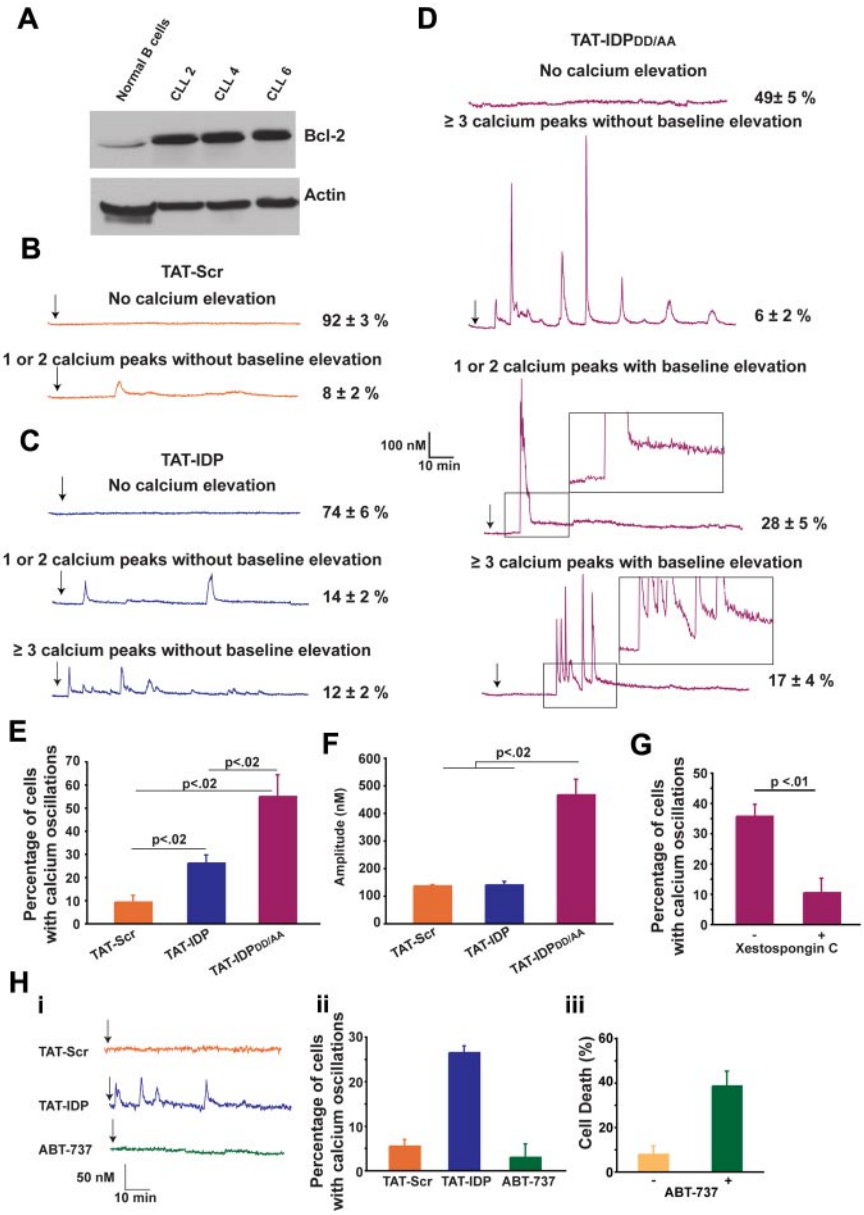

Figure 5. Peptide-induced Ca^{2+} oscillations in primary CLL cells. (A) Immunoblot comparing Bcl-2 levels in normal human B lymphocytes and 3 primary CLL samples. (B-D) Representative single-cell Ca^{2+} recordings illustrating the Ca^{2+} responses observed in CLL cells after addition (arrow) of 10μM of each peptide shown. Portions of the traces in panel D are magnified (insets) to illustrate the baseline Ca^{2+} elevation induced by TAT-$IDP_{DD/AA}$. (E) Percentage of CLL cells displaying Ca^{2+} oscillations in response to 10μM peptide addition during 90 minutes of single-cell recordings (mean ± SE, 3 experiments each using CLL cells isolated from a different patient, average 85 cells per experiment). (F) Amplitude of individual Ca^{2+} spikes in the same experiments shown in panel E (mean ± SE). (G) Inhibition of peptide-induced Ca^{2+} oscillations by xestospongin C summarized as percentage of CLL cells displaying Ca^{2+} oscillations during 90 minutes of single-cell recordings after the addition of TAT-$IDP_{DD/AA}$ (5-10μM); cells were pretreated for 30 minutes with either DMSO (−) or 10μM xestospongin C (+) (mean ± SE, 4 experiments, average 75 cells analyzed per recording). (H) Failure of ABT-737 to induce Ca^{2+} elevation: (i) representative single-cell Ca^{2+} recordings in CLL cells, with arrow designating addition of 5μM TAT-Scr or TAT-IDP or 2μM ABT-737; (ii) percentage of CLL cells with Ca^{2+} oscillations in response to 5μM TAT-Scr or TAT-IDP or 2μM ABT-737, with symbols representing the mean ± SE in 2 experiments (average 80 cells per experiment); (iii) cell death (trypan blue dye uptake) in CLL cells incubated with or without 2μM ABT-737 for 24 hours, with symbols representing the mean ± SE in 7 experiments (average 400 cells counted per individual treatment).

associated with an elevated level of Bcl-2 and because Bcl-2 plays an important role in apoptosis resistance in this disease. CLL cells were isolated from the peripheral blood of untreated patients. Malignant lymphocytes, which represented more than 80% of lymphocytes in peripheral blood samples, were separated by density gradient separation and used immediately in experiments without interval storage. The relatively high level of Bcl-2 in CLL cells compared with that in normal B lymphocytes is presented in Figure 5A and is representative of the CLL samples used here. The patterns of Ca^{2+} elevation induced by TAT-Scr, TAT-IDP, and TAT-$IDP_{DD/AA}$ in CLL cells are illustrated by representative single-cell traces in Figure 5B-D and are summarized quantitatively in Figure 5E. Less than 10% of untreated cells (not shown) or TAT-Scr–treated cells had detectable Ca^{2+} elevations in recordings that were typically 90 minutes in duration. TAT-IDP induced Ca^{2+} elevation in only 26% ± 2% of CLL cells, corresponding to either single or dual spikes (14% ± 2%) or repetitive oscillations (≥ 3 successive Ca^{2+} spikes; 12% ± 2%). Thus, overall Ca^{2+} responses to TAT-IDP were much less than those observed in the cell lines investigated in this study. On the other hand, TAT-$IDP_{DD/AA}$ induced Ca^{2+} elevation in 51% ± 5% of CLL cells isolated from 7 patients.

The response patterns and percentages of responses were remarkably similar among the individual patient samples. Several different patterns of Ca^{2+} elevation were observed in CLL cells after TAT-$IDP_{DD/AA}$ addition (Figure 5D). One pattern, observed in only 6% ± 2% of cells, consisted of prolonged Ca^{2+} oscillations without baseline Ca^{2+} elevation, similar to the patterns observed previously in Bcl-2–positive cell lines described above in Figure 2. The more prominent patterns included 1 or 2 high-amplitude spikes associated with prolonged basal Ca^{2+} elevation (28% ± 5% of cells) or a relatively brief burst of Ca^{2+} oscillations, also associated with prolonged basal Ca^{2+} elevation (17% ± 4% of cells). Analysis of multiple experiments monitoring Ca^{2+} responses in a large number of cells documented that differences in the relative abilities of TAT-Scr, TAT-IDP, and TAT-$IDP_{DD/AA}$ to induce Ca^{2+} elevations were highly significant (Figure 5E). In addition,

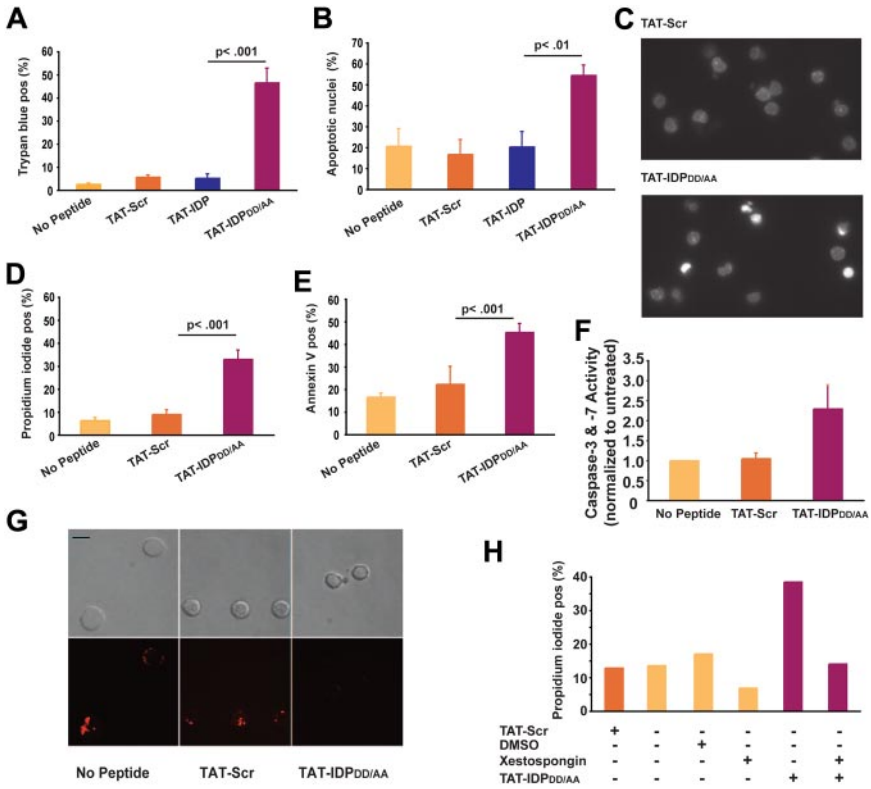

Figure 6. Peptide-induced apoptosis in primary CLL cells. (A) CLL cells from 8 patients were treated with 10μM of each peptide shown and the percentage of dead cells, identified by trypan blue dye uptake, was determined 24 hours later; results are presented as mean ± SE. (B) CLL cells from 4 different patients were treated with 10μM of each peptide shown, and 24 hours later the percentage of cells (mean ± SE) with typical apoptotic morphology was determined by fluorescence microscopic analysis of Hoechst-stained nuclei. (C) Images of Hoechst-stained nuclei illustrating apoptotic morphology 24 hours after treatment with 10μM TAT-IDP$_{DD/AA}$. (D) Experiments using CLL cells from 6 patients to quantify the percentage of dead cells (mean ± SE) by flow cytometric analysis of propidium iodide uptake 24 hours after treatment with 10μM of the peptides shown. (E) Flow cytometric analysis of the same samples shown in panel D quantifying the percentage of annexin V–positive cells (mean ± SE) 24 hours after treatment with 10μM of the peptides shown. (F) Caspase-3/7 activation induced by TAT-IDP$_{DD/AA}$ (mean ± SE, 2 experiments). (G) Representative confocal images of CLL cells loaded with TMRM, indicating loss of mitochondrial membrane potential 24 hours after adding TAT-IDP$_{DD/AA}$. Top panels are bright-field images; bottom panels are fluorescence images. Bar = 8 μm. (H) Inhibition of TAT-IDP$_{DD/AA}$–induced CLL cell death by xestospongin C (10μM) added 30 minutes before peptides, based on analysis of 85 cells, representative of 3 experiments using CLL cells from different patients.

the amplitude of Ca^{2+} peaks was significantly higher after TAT-IDP$_{DD/AA}$ compared with TAT-IDP (Figure 5F). While differing in pattern and amplitude, the Ca^{2+} responses to both TAT-IDP (data not shown) and TAT-IDP$_{DD/AA}$ were inhibited by xestospongin C, which is consistent with a role of IP$_3$R-mediated Ca^{2+} release in the initiation of Ca^{2+} elevations by both peptides (Figure 5G).

In contrast to peptide-induced Ca^{2+} elevation, the BH3-mimetic ABT-737 did not induce Ca^{2+} elevation in CLL cells, even though ABT-737 induced the death of 40% of CLL cells at 24 hours (Figure 5H). This latter finding underscores the difference in mechanism between ABT-737 and peptides designed to inhibit Bcl-2 binding to the IP$_3$R (see "Discussion"). In summary, the findings shown in Figure 5 indicate that TAT-IDP$_{DD/AA}$ induces significant Ca^{2+} elevation in primary CLL cells, and that the pattern of Ca^{2+} elevation is different from that elicited by TAT-IDP$_{DD/AA}$ in Bcl-2–positive cell lines. Two main differences were detected: (1) TAT-IDP$_{DD/AA}$ induced only a brief period of Ca^{2+} spiking rather than prolonged Ca^{2+} oscillations, and (2) after TAT-IDP$_{DD/AA}$ addition, the brief period of Ca^{2+} spiking in CLL cells was followed by a continuous cytoplasmic Ca^{2+} elevation that was not observed in the cell lines.

TAT-IDP$_{DD/AA}$-evoked Ca^{2+} elevation induces apoptosis in primary CLL cells but not in normal lymphocytes

Because continuous cytoplasmic Ca^{2+} elevation can trigger apoptosis and necrosis, the effects of TAT-IDP$_{DD/AA}$ on CLL-cell viability were tested. As shown in Figure 6, TAT-IDP$_{DD/AA}$-mediated Ca^{2+} elevation induced substantial apoptosis in CLL cells. This was observed consistently in CLL samples isolated from 8 patients. Cell death was documented by trypan blue dye uptake (Figure 6A) and propidium iodide uptake (Figure 6D), while apoptosis induction was documented by observing apoptotic nuclear morphology (Figure 6B-C) and by detecting phosphatidylserine exposure on the cell surface with annexin V (Figure 6E). Consistent with these findings, TAT-IDP$_{DD/AA}$ treatment activated caspases (Figure 6F) and caused loss of mitochondrial membrane potential (Figure 6G). The induction of cell death was specific to TAT-IDP$_{DD/AA}$, because neither TAT-Scr nor TAT-IDP induced apoptosis in CLL cells. Moreover, apoptosis induction by TAT-IDP$_{DD/AA}$ was inhibited by xestospongin C, confirming that TAT-IDP$_{DD/AA}$-induced apoptosis was IP$_3$R mediated (Figure 6H). Because IP$_3$R-mediated apoptosis is triggered by Ca^{2+} elevation,[19,20] we inferred that Ca^{2+} elevation is the initiating factor in TAT-IDP$_{DD/AA}$-induced apoptosis. Ideally, intracellular Ca^{2+} chelators (eg, BAPTA-AM) would be used to suppress Ca^{2+} elevation and thereby directly confirm the role of Ca^{2+} elevation in TAT-IDP$_{DD/AA}$-induced apoptosis. However, this is not possible because buffering intracellular Ca^{2+} with BAPTA-AM kills CLL cells (F. Z., unpublished observations), ostensibly by inhibiting the basal Ca^{2+} signals required for cell survival. CLL cells were more than 6-fold more sensitive to apoptosis induced by TAT-IDP$_{DD/AA}$ than normal peripheral blood lymphocytes (Figure 7A-B), suggesting that TAT-IDP$_{DD/AA}$ may selectively target leukemia cells that overexpress Bcl-2.

Discussion

The findings reported here provide novel insight into the role of Bcl-2 in the pathogenesis of CLL, and suggest that it may be worthwhile to target the Bcl-2–IP$_3$R interaction therapeutically. The present undertaking was fostered by the unexpected discovery that IDP by itself (ie, without an external IP$_3$-generating stimulus

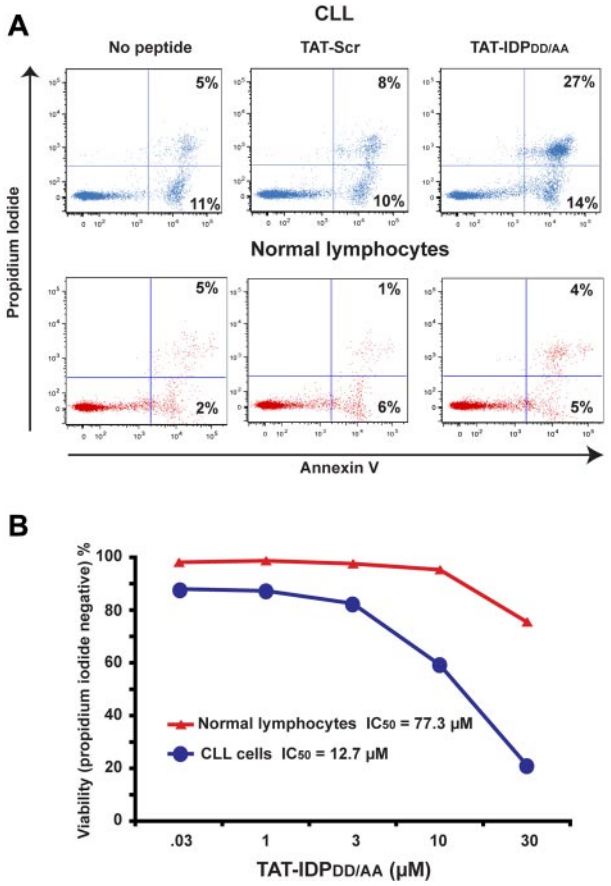

Figure 7. Peptide-induced apoptosis in primary CLL cells but not in normal lymphocytes. (A) Flow cytometric representations comparing proportions of CLL cells and normal human lymphocytes that are both propidium iodide positive and annexin V positive 24 hours after addition of 10μM TAT-Scr or TAT-IDP$_{DD/AA}$. (B) Dose-response curves comparing viability of CLL cells versus normal lymphocytes based on flow cytometric quantification of propidium iodide exclusion 24 hours after adding TAT-IDP$_{DD/AA}$. Results are representative of 2 side-by-side comparisons using CLL cells and normal cells from different donors.

such as anti-CD3–mediated T-cell receptor [TCR] activation) induces Ca^{2+} elevation when introduced in Bcl-2–positive leukemia/lymphoma cells. IDP induced Ca^{2+} elevation regardless of its mode of delivery into cells (ie, as a TAT fusion peptide or using Chariot peptide uptake reagent). The recognition of a potential aspartyl cleavage site within the IDP sequence prompted the modification of TAT-IDP to TAT-IDP$_{DD/AA}$. Both peptides induce IP_3R-dependent Ca^{2+} elevation by binding to the BH4 domain of Bcl-2 and thereby disrupting the Bcl-2–IP_3R interaction, but TAT-IDP$_{DD/AA}$ induces Ca^{2+} elevations of higher frequency and amplitude than observed with IDP itself, ostensibly because it is less subject to degradation during endocytic uptake (in vitro biochemical studies indicate a similar affinity of IDP and TAT-IDP$_{DD/AA}$ for Bcl-2).

Although peptide-mediated disruption of the Bcl-2–IP_3R interaction induced Ca^{2+} elevation both in cell lines and in primary CLL cells, the patterns of Ca^{2+} elevation were different. In each of the cell lines, the predominant pattern was oscillatory, composed of periodic Ca^{2+} spikes. A similar oscillatory pattern was induced in CLL cells by TAT-IDP, whereas in CLL cells, TAT-IDP$_{DD/AA}$ initially induced high-amplitude Ca^{2+} elevations (either 1 or 2 transient elevations or a brief burst of Ca^{2+} oscillations), followed by a sustained elevation of Ca^{2+} above basal levels. These differences in the pattern of Ca^{2+} elevation were highly reproducible and correlated with different outcomes of peptide treatment. TAT-IDP and TAT-IDP$_{DD/AA}$ did not induce cell death in the cell lines, nor did TAT-IDP induce cell death in primary CLL cells. In contrast, TAT-IDP$_{DD/AA}$ induced apoptosis in primary CLL cells. These findings are reminiscent of the earlier observation that Ca^{2+} oscillations induced by TCR stimulation do not induce apoptosis, whereas apoptosis ensues after strong TCR activation sufficient to induce Ca^{2+} elevation that is of high amplitude and continuous rather than oscillatory.[22] Overall, these observations are consistent with the known prosurvival functions of Ca^{2+} oscillations, including stimulation of mitochondrial metabolism, whereas sustained high-amplitude elevations of Ca^{2+} trigger apoptosis, in part by overloading mitochondria with Ca^{2+} and thus decreasing mitochondrial membrane potential.[40-45] Further investigation will be required to fully understand the nature of these differences in the Ca^{2+}-signaling pattern. Moreover, continued work will be required to fully understand the detailed mechanism by which TAT-IDP$_{DD/AA}$ induces apoptosis in primary CLL cells. Nevertheless, this mechanism is likely to involve the intrinsic, Bax/Bak-dependent apoptotic pathway, because Ca^{2+} elevation is known to trigger this cell-death pathway by either activating or inducing the expression of Bad and Bim, BH3 members of the Bcl-2 protein family.[19,20]

Remodeling of Ca^{2+} homeostasis and signaling through a variety of mechanisms supports the survival and proliferation of cancer cells.[21] The findings reported here suggest that the interaction of Bcl-2 with IP_3R may contribute to this remodeling process by repressing Ca^{2+} signals driven by tonic BCR signaling, a hallmark of CLL pathogenesis.[6,46-48] Therefore, because BCR signaling increases IP_3 synthesis by activating phospholipase C, exposure of CLL cells to TAT-IDP$_{DD/AA}$ alone would be sufficient to expose these Ca^{2+} signals by displacing Bcl-2 from IP_3R. The capacity of TAT-IDP$_{DD/AA}$ to induce Ca^{2+}-mediated apoptosis raises the prospect of targeting the Bcl-2–IP_3R interaction for therapeutic purposes in CLL and other Bcl-2–positive malignancies. The concept of targeting the Bcl-2–IP_3R interaction for therapeutic purposes is supported by evidence that TAT-IDP$_{DD/AA}$ induces apoptosis in primary CLL cells, but not in normal lymphocytes.

Based on the proposed key role of BCR signaling in the pathogenesis of CLL, novel therapeutic approaches are being directed at various elements of the BCR-signaling pathway, including BCR-associated kinases such as Lyn and ZAP-70 and BCR regulatory molecules such as CD19 and CD20.[6] Bcl-2, which is almost invariably elevated in CLL, is a prime therapeutic target. A considerable amount of effort is currently being directed toward inhibiting Bcl-2, based on understanding the Bcl-2 mechanism at a structure-function level.[1,2,11] A major target is the hydrophobic groove formed by the BH1, BH2, and BH3 domains of Bcl-2, in which the BH3 domains of proapoptotic Bcl-2 family members bind. BH3-mimetics, such as ABT-737, are modeled to fit in this groove, thus liberating proapoptotic proteins from Bcl-2 and thereby inducing apoptosis.[9,49,50] Other Bcl-2 inhibitors trigger cell death but, unlike ABT-737, their mode of cell-death induction is independent of Bax/Bak activation.[51] On the other hand, TAT-IDP$_{DD/AA}$ binds to the BH4 domain, displacing Bcl-2 from IP_3R and inducing apoptosis by a Ca^{2+}-dependent mechanism disparate from that of ABT-737, which does not elevate Ca^{2+}. Therefore, the disruption of the Bcl-2–IP_3R interaction represents a unique strategy with which to target CLL therapeutically, and is different from approaches that inhibit upstream components of the BCR-signaling pathway and from strategies that interrupt the binding of proapoptotic proteins by Bcl-2.

Acknowledgments

We thank Stephen Tahir, Abbott Laboratories, for providing ABT-737, and Michael Berridge, Martin Bootman, Zhenghe John Wang, and Andrew Lavik for helpful suggestions regarding the manuscript.

This work was supported by National Institutes of Health grants RO1 CA085804 (to C.W.D.), T32 CA059366 (M.W.H.), T32 HL007147 (J.K.M.), T32 GM08803-02 (C.R.) and T32 GM007250 (to J.K.M. and C.R.). Research performed at the K.U. Leuven was supported by Research Program G.0604.07 of the Research Foundation-Flanders (FWO), by grant GOA/09/012 of the Concerted Actions Program of the K.U. Leuven (to J.B.P. and H.D.S.), and by Onderzoekstoelage grant STRT1/10/044 of the K.U. Leuven (to G.B.). G.M. is the recipient of a doctoral fellowship from the FWO.

Contributions: F.Z. performed research, analyzed and interpreted data; M.W.H. performed research, analyzed and interpreted data, and wrote the manuscript; G.B. performed research, analyzed and interpreted data, and wrote the manuscript; G.M. performed research, analyzed and interpreted data; J.B.P. provided valuable new reagents, analyzed and interpreted data, and wrote the manuscript; and H.D.S. provided valuable new reagents, analyzed and interpreted data, and wrote the manuscript; Y.R. performed research; J.K.M. performed research, analyzed and interpreted data; M.L. performed research; C.R. analyzed and interpreted data; S.M. analyzed and interpreted data; and C.W.D. designed research, analyzed and interpreted data, performed statistical analysis, and wrote the manuscript.

Conflict of interest disclosure: The authors declare no competing financial interests.

Correspondence: Clark W. Distelhorst, MD, Charles S. Britton II Professor of Hematology/Oncology, Case Western Reserve University School of Medicine, 10900 Euclid Ave, Cleveland, OH 44106; e-mail: cwd@case.edu.

References

1. Adams JM, Cory S. The Bcl-2 apoptotic switch in cancer development and therapy. *Oncogene.* 2007;26(9):1324-1337.
2. Yip KW, Reed JC. Bcl-2 family proteins and cancer. *Oncogene.* 2008;27(50):6398-6406.
3. Tsujimoto Y, Finger LR, Yunis J, Nowell PC, Croce CM. Cloning of the chromosome breakpoint of neoplastic B cells with the t(14;18) chromosome translocation. *Science.* 1984;226(4678): 1097-1099.
4. Cimmino A, Calin GA, Fabbri M, et al. miR-15 and miR-16 induce apoptosis by targeting BCL2. *Proc Natl Acad Sci U S A.* 2005;102(39):13944-13949.
5. Calin GA, Croce C. Chronic lymphocytic leukemia: interplay between noncoding RNAs and protein-coding genes. *Blood.* 2009;114(23):4761-4770.
6. Pleyer L, Egle A, Hartmann TN, Greil R. Molecular and cellular mechanisms of CLL: novel therapeutic approaches. *Nat Rev Clin Oncol.* 2009; 6(7):405-418.
7. Youle RJ, Strasser A. The Bcl-2 protein family: opposing activities that mediate cell death. *Nat Rev Mol Cell Biol.* 2008;9(1):47-59.
8. Chipuk JE, Moldoveanu T, Llambi F, Parsons MJ, Green DR. The BCL-2 family reunion. *Mol Cell.* 2010;37(3):299-310.
9. Letai AG. Diagnosing and exploiting cancer's addiction to blocks in apoptosis. *Nat Rev Cancer.* 2008;8(2):121-132.
10. Warr MR, Shore GC. Small-molecule Bcl-2 antagonists as targeted therapy in oncology. *Curr Oncol.* 2008;15(6):256-261.
11. Vogler M, Dinsdale D, Dyer MJ, Cohen GM. Bcl-2 inhibitors: small molecules with a big impact on cancer therapy. *Cell Death Differ.* 2009;16(3): 360-367.
12. Pinton P, Rizzuto R. Bcl-2 and Ca2+ homeostasis in the endoplasmic reticulum. *Cell Death Differ.* 2006;13(8):1409-1418.
13. Heath-Engel HM, Chang NC, Shore GC. The endoplasmic reticulum in apoptosis and autophagy: role of the Bcl-2 protein family. *Oncogene.* 2008; 27(50):6419-6433.
14. Rong Y, Distelhorst CW. Bcl-2 protein family: Versatile regulators of calcium signaling in cell survival and apoptosis. *Annu Rev Physiol.* 2008;70: 73-91.
15. Bezprozvanny I. The inositol 1,4,5-trisphosphate receptors. *Cell Calcium.* 2005;38(3-4):261-272.
16. Foskett JK, White C, Cheung KH, Mak DO. Inositol trisphosphate receptor Ca2+ release channels. *Physiol Rev.* 2007;87(2):593-658.
17. Berridge MJ, Bootman MD, Roderick HL. Calcium signaling: dynamics, homeostasis and remodelling. *Nat Rev Mol Cell Biol.* 2003;4(7):517-529.
18. Lewis RS. Calcium signaling mechanisms in T lymphocytes. *Annu Rev Immunol.* 2001;19:497-521.
19. Orrenius S, Zhivotovsky B, Nicotera P. Regulation of cell death: The calcium-apoptosis link. *Nat Rev Mol Cell Biol.* 2003;4(7):552-565.
20. Joseph SK, Hajnoczky G. IP3 receptors in cell survival and apoptosis: Ca2+ release and beyond. *Apoptosis.* 2007;12(5):951-968.
21. Roderick HL, Cook SJ. Ca2+ signalling checkpoints in cancer: remodelling Ca2+ for cancer cell proliferation and survival. *Nat Rev Cancer.* 2008;8(5):361-365.
22. Zhong F, Davis MC, McColl KS, Distelhorst CW. Bcl-2 differentially regulates Ca2+ signals according to the strength of T cell receptor activation. *J Cell Biol.* 2006;172(1):127-137.
23. Palmer AE, Jin C, Reed JC, Tsien RY. Bcl-2–mediated alterations in endoplasmic reticulum Ca2+ analyzed with an improved genetically encoded fluorescent sensor. *Proc Natl Acad Sci U S A.* 2004;101(50):17404-17409.
24. White C, Li C, Yang J, et al. The endoplasmic reticulum gateway to apoptosis by Bcl-XI modulation of the InsP3R. *Nat Cell Biol.* 2005;7(10): 1021-1028.
25. Li C, Wang X, Vais H, Thompson CB, Foskett JK, White C. Apoptosis regulation by Bcl-XL modulation of mammalian inositol 1,4,5-trisphosphate receptor channel isoform gating. *Proc Natl Acad Sci U S A.* 2007;104(30):12565-12570.
26. Eckenrode EF, Yang J, Velmurugan GV, Foskett JK, White C. Apoptosis protection by Mcl-1 and Bcl-2 modulation of inositol 1,4,5-trisphosphate receptor-dpendent Ca2+ signaling. *J Biol Chem.* 2010;285(18):13678-13684.
27. Cárdenas C, Miller RA, Simth I, et al. Essential regulation of cell bioenergetics by constitutive InsP3 receptor Ca2+ transfer to mitochondria. *Cell.* 2010;142(2):270-283.
28. Chen R, Valencia I, Zhong F, et al. Bcl-2 functionally interacts with inositol 1,4,5-trisphosphate receptors to regulate calcium release from the ER. *J Cell Biol.* 2004;166(2):193-203.
29. Oakes SA, Scorrano L, Opferman JT, et al. Proapoptotic BAX and BAK regulate the type 1 inositol trisphosphate receptor and calcium leak from the endoplasmic reticulum. *Proc Natl Acad Sci U S A.* 2005;102(1):105-110.
30. Basset O, Boittin F-X, Cognard C, Constantin B, Ruegg UT. Bcl-2 overexpression prevents calcium overload and subsequent apoptosis in dystrophic myotubes. *Biochem J.* 2006;395(2):267-276.
31. Xu L, Kong D, Zhu L, Zhu W, Andrews DW, Kuo TH. Suppression of IP3-mediated calcium release and apoptosis by Bcl-2 involves the participation of protein phosphatase 1. *Mol Cell Biochem.* 2007;295(1-2):153-165.
32. Hanson CJ, Bootman MD, Distelhorst CW, Wojcikiewicz RJ, Roderick HL. Bcl-2 suppresses Ca2+ release through inositol 1,4,5-trisphosphate receptors and inhibits Ca2+ uptake by mitochondria without affecting ER calcium store content. *Cell Calcium.* 2008;44(3):324-338.
33. Rong Y, Aromolaran AS, Bultynck G, et al. Targeting Bcl-2–IP3 receptor interaction to reverse Bcl-2's inhibition of apoptotic calcium signals. *Mol Cell.* 2008;31(2):255-265.
34. Rong Y, Bultynck G, Aromolaran AS, et al. The BH4 domain of Bcl-2 inhibits ER calcium release and apoptosis by binding the regulatory and coupling domain of the IP3 receptor. *Proc Natl Acad Sci U S A.* 2009;106(34):14397-14402.
35. Kasri NN, Kocks SL, Verbert L, et al. Up-regulation of inositol 1,4,5-trisphosphate receptor type 1 is responsible for a decreased endoplasmic-reticulum Ca2+ content in presenilin double knockout cells. *Cell Calcium.* 2006;40(1):41-51.
36. Wadia JS, Stan RV, Dowdy SF. Transducible TAT-HA fusogenic peptide enhances escape of TAT-fusion proteins after lipid raft macropinocytosis. *Nat Med.* 2004;10(3):310-315.
37. Reich M, van Swieten PF, Sommandas V, et al. Endocytosis targets exogenous material selectively to cathepsin S in live human dendritic cells, while cell penetrating peptides mediate nonselective transport to cystein cathepsins. *J Leukoc Biol.* 2007;81(4):990-1001.
38. Wee LJ, Tan TW, Ranganathan S. SVM-based prediction of caspase substrate cleavage sites. *BMC Bioinformatics.* 2006;7(suppl 5):S14.
39. Kitada S, Andersen J, Akar S, et al. Expression of apoptosis-regulating proteins in chronic lymphocytic leukemia: correlations with in vitro and in vivo chemoresponses. *Blood.* 1998;91(9):3379-3389.
40. Rizzuto R, Pinton P, Carrington W, et al. Close contacts with the endoplasmic reticulum as determinants of mitochondrial Ca2+ responses. *Science.* 1998;280(5370):1763-1766.
41. Szalai G, Krishnamurthy R, Hajnoczky G. Apoptosis driven by IP(3)-linked mitochondrial calcium signals. *EMBO J.* 1999;18(22):6349-6361.

42. Pacher P, Hajnoczky G. Propagation of the apoptotic signal by mitochondrial waves. *EMBO J.* 2001;20(15):4107-4121.

43. Csordás G, Renken C, Varnai P, et al. Structural and functional features and significance of the physical linkage between ER and mitochondria. *J Cell Biol.* 2006;174(7):915-921.

44. Giacomello M, Drago I, Pizzo P, Pozzan T. Mitochondrial Ca2+ as a key regulator of cell life and death. *Cell Death Differ.* 2007;14(7):1267-1274.

45. Rizzuto R, Pozzan T. Microdomains of intracellular Ca2+: Molecular determinants and functional consequences. *Physiol Rev.* 2006;86(1):369-408.

46. Contri A, Brunati AM, Trentin L, et al. Chronic lymphocytic leukemia B cells contain anomalous Lyn tyrosine kinase, a putative contribution to defective apoptosis. *J Clin Invest.* 2005;115(2):369-378.

47. Petlickovski A, Laurenti L, Li X, et al. Sustained signaling through the B-cell receptor induces Mcl-1 and promotes survival of chronic lymphocytic leukemia B cells. *Blood.* 2005;105(12):4820-4827.

48. Cozma D, Yu D, Hodawadekar S, et al. B cell activator PAX5 promotes lymphomagenesis through stimulation of B-cell receptor signaling. *J Clin Invest.* 2007;117(9):2602-2610.

49. Oltersdorf T, Elmore SW, Shoemaker AR, et al. An inhibitor of Bcl-2 family proteins induces regression of solid tumours. *Nature.* 2005; 435(7042):677-681.

50. Del Gaizo Moore V, Brown JR, Certo M, Love TM, Novina CD, Letai A. Chronic lymphocytic leukemia requires BCL2 to sequester prodeath BIM, explaining sensitivity to BCL2 antagonist ABT-737. *J Clin Invest.* 2007;117(1):112-121.

51. Vogler M, Dinsdale D, Sun XM, et al. A novel paradigm for rapid ABT-737-induced apoptosis involving outer mitochondrial membrane rupture in primary leukemia and lymphoma cells. *Cell Death Differ.* 2008;15(5):820-830.